



1 **Measurement of Light absorbing particles in surface snow of**  
2 **central and western Himalayan glaciers: spatial variability,**  
3 **radiative impacts, and potential source regions**

4

5

6 Chaman Gul<sup>1,2,3,4</sup>, Shichang Kang<sup>1,4</sup>, Siva Praveen Puppala<sup>2</sup>, Xiaokang Wu<sup>5</sup>, Cenlin He<sup>6</sup>,  
Yangyang Xu<sup>5</sup>, Inka Koch<sup>1</sup>, Sher Muhammad<sup>1</sup>, Rajesh Kumar<sup>6</sup>, Getachew Dubache<sup>3</sup>

7

8 <sup>1</sup>State Key Laboratory of Cryosphere Science, Northwest Institute of Eco-Environment and Resources, Chinese  
9 Academy of Sciences, Lanzhou 73000, China

10 <sup>2</sup>International Centre for Integrated Mountain Development (ICIMOD), G.P.O. Box 3226, Kathmandu, Nepal

11 <sup>3</sup>Reading Academy, Nanjing University of Information Sciences and Technology 219 Ningliu Road, Nanjing,  
12 Jiangsu, 210044 China.

13 <sup>4</sup>University of Chinese Academy of Sciences, Beijing, China

14 <sup>5</sup>Department of Atmospheric Sciences, Texas A&M University, College Station, TX 77843, USA

15 <sup>6</sup>Research Applications Laboratory, National Center for Atmospheric Research, Boulder, CO 80301, USA

16

17

18

19

20 Correspondence: Siva Praveen Puppala ([sivapraveen.puppala@icimod.org](mailto:sivapraveen.puppala@icimod.org));

21

22



23 **Abstract.** We collected surface snow samples from three different glaciers: Yala, Thana, and Sachin in the central  
24 and western Himalayas to understand the spatial variability and radiative impacts of light-absorbing particles. The  
25 Yala and Thana glaciers in Nepal and Bhutan, respectively, were selected to represent the central Himalayas. The  
26 Sachin glacier in Pakistan was selected to represent the western Himalayas. The samples were collected during the  
27 pre-and post-monsoon seasons of the year 2016. The samples were analysed for black carbon (BC) and water-  
28 insoluble organic carbon (OC) through the thermal optical method. The average mass concentrations (BC 2381.39  
29  $\text{ng g}^{-1}$ ; OC 3896.00  $\text{ng g}^{-1}$ ; dust 101.05  $\mu\text{g g}^{-1}$ ) in the western Himalaya (Sachin glacier) were quite higher compared  
30 to the mass concentrations (BC 357.93  $\text{ng g}^{-1}$ , OC 903.86  $\text{ng g}^{-1}$ , dust 21.95  $\mu\text{g g}^{-1}$ ) at the central Himalaya (Yala  
31 glacier). The difference in mass concentration may be due to the difference in elevation, snow age, local pollution  
32 sources, and difference in meteorological conditions. BC in surface snow was also estimated through WRF-Chem  
33 simulations at the three glacier sites during the sampling periods. Simulations reasonably capture the spatial and  
34 seasonal patterns of the observed BC in snow but with a relatively smaller magnitude. Absolute snow albedo was  
35 estimated through the Snow, Ice, and Aerosol Radiation (SNICAR) model. The absolute snow albedo reduction was  
36 ranging between 0.48 % (Thana glacier during September) to 24 % (Sachin glacier during May) due to BC and 0.13  
37 % (Yala glacier during September) to 5% (Sachin glacier during May) due to dust. The instantaneous radiative  
38 forcing due to BC and dust was estimated in the range of 0 to 96.48  $\text{W m}^{-2}$  and 0 to 25  $\text{W m}^{-2}$  respectively. The  
39 lowest and highest albedo reduction and radiative forcing were observed in central and western Himalayan glaciers,  
40 respectively. The potential source regions of the deposited pollutants were inferred using WRF-Chem tagged-tracer  
41 simulations. Selected glaciers in the western Himalayas were mostly affected by long-range transport from the  
42 Middle East and Central Asia; however, the central Himalayan glaciers were mainly affected by local and South  
43 Asia emissions (from Nepal, India, and China) especially during the pre-monsoon season. Overall, South Asia and  
44 West Asia were the main contributing source regions of pollutants.

45

46 **Keywords:** black carbon; organic carbon; Yala glacier; Thana glacier; Sachin glacier; snow albedo

47

48



## 49 1 Introduction

50 Black carbon (BC) is a distinct type of carbonaceous material that is formed primarily in flames. BC particles in the  
51 atmosphere are generally produced by the incomplete combustion of fossil fuel, biofuel, and biomass. BC is only a  
52 minor contributor to aerosol mass but has great climatic interest as a strong absorber of solar radiation (Quinn et al.,  
53 2008; Ramanathan and Carmichael, 2008). In addition to warming, BC particles can interact with clouds, changing  
54 their microphysical properties, and thus impacting the climate (Wang et al., 2018; Bond et al., 2013; Dong et al.,  
55 2021). Besides this, several studies in the past highlighted the role of BC on the cryosphere (Kang et al., 2019,  
56 2020).

57

58 The cryosphere is one of the most sensitive indicators of climate change. The temperature rise in cryospheric regions  
59 is generally larger than that in other regions on the global scale (Pepin and Lundquist 2008; Kang et al., 2010; You  
60 et al., 2021; Huang et al., 2019). BC particles deposit on the glaciers or snow cover surface, decreasing the surface  
61 albedo and absorbing more solar radiation (Warren and Brandt, 2008; He et al., 2017) which accelerates snow and  
62 ice melt and triggering albedo feedback (Flanner et al., 2009; Hansen and Nazarenko, 2004; Kang et al., 2020). The  
63 forcing produced by BC and other light-absorbing particles (LAPs) further affects the regional climate (Flanner et  
64 al., 2009; Xu et al., 2016; Ji et al., 2015) leads to complex responses of the Earth climate system (Hansen et al.,  
65 1997). The largest climate forcing from BC in the snow is estimated to occur over the Tibetan Plateau (TP) and  
66 Himalayas (Flanner et al., 2009; Ji et al., 2015).

67

68 Mountain glaciers are the most important freshwater resources to the lives of arid and semi-arid regions (Hock,  
69 2005, 19; Mayer et al., 2006). The great Himalayas is considered as world's largest freshwater reservoir outside the  
70 Polar Regions (Immerzeel et al., 2010; Marcovecchio et al., 2021). The economy and lives of millions of people in  
71 the region are influenced by the changes in mountain river discharge downstream of the Himalayas (Vaux et al.,  
72 2012). Lack of in-situ data, the low resolution of emission inventory, and coarse model resolutions prevent an  
73 accurate evaluation of LAPs impacts on snow albedo and radiative forcing. Many glaciers have retreated in the  
74 region due to climate warming (Zhang et al., 2009; Kang et al., 2010; Yao et al., 2019), and possibly due to LAP-  
75 induced surface darkening (Flanner et al., 2009; Qian et al., 2011; Kang et al., 2019). Glacier retreat in the TP and  
76 the Himalayan region has serious consequences because snow and runoff from this region are sources of major  
77 rivers in Asia, and the availability of freshwater resources has profound effects on human health and agriculture  
78 (Immerzeel et al., 2010). However, it is still large uncertainties for glacier retreat driven predominately by the  
79 deposition of BC and other LAPs (Bolch et al., 2012; Kang et al., 2020).

80

81 Snow albedo is an important indicator of surface energy budget over the snow-covered area. Small changes in  
82 surface snow albedo can have large impacts on surface warming due to the rapid feedbacks involving changes to  
83 sublimation, snow morphology, and melt rates (Bond et al., 2013). The concentration of LAPs in surface snow is a  
84 major factor that affects snow albedo. BC and other LAPs present in the snow reduce the albedo in the visible  
85 portion of the electromagnetic spectrum (e.g., Warren and Wiscombe, 1980, Flanner et al., 2007). Besides the



86 concentration of pollutants deposited on the surface of the snow, multiple other factors, such as solar zenith angle  
87 (SZA), snow grain size, snow shape, snow texture, snow density, and snowpack thickness, can also affect snow  
88 albedo (He and Flanner, 2020). The radiative transfer model used for the albedo has brought a better understanding  
89 of snow optical properties in the shortwave spectrum (He and Flanner, 2020). We estimated the spectral snow  
90 albedo using the online Snow, Ice, and Aerosol Radiative (SNICAR) model (Flanner and Zender, 2006). The model  
91 was originally developed by Flanner et al., 2007, further updated by He et al. (2018) and Dang et al., (2019), and has  
92 been widely used in simulating the impacts of LAPs on snow albedos (Qu et al., 2014).

93  
94 Here we present the mass concentration of BC, water-insoluble organic carbon (OC), and mineral dust in surface  
95 snow from the ablation and accumulation zones of selected glaciers, located in three different countries (Nepal,  
96 Bhutan, and Pakistan) on the southern slope of the Himalaya. The Yala and Thana glaciers were selected from the  
97 central Himalayas, while the Sachin glacier was selected from the western Himalayas. To reasonably compare the  
98 results (mass concentrations, and optical and radiative properties) across the central and western Himalayas, samples  
99 were collected on similar dates of the same seasons (pre-monsoon and post-monsoon). We investigate the spatial  
100 variability of BC, OC, and mineral dust concentrations due to differences in the source region, meteorology,  
101 deposition, and post-deposition processes. The measured mass concentrations were compared to regional model  
102 simulations. The associated changes in surface snow albedo and radiative forcing (RF) by mineral dust and BC in  
103 surface snow were estimated using the SNICAR model. We also aim to identify the potential source regions of  
104 pollution reaching sampling sites using tracer-tagged model simulations.

105

## 106 **2 Study area and meteorology**

107 Samples were collected from the Yala glacier (28°14' N, 85°37' E) in the Langtang valley of Nepal, the Thana  
108 glacier (28°01' N, 90°36' E) in the Chamkhar valley of Bhutan, and the Sachin glacier (35°19' N, 74°45' E) in  
109 northern Pakistan (Table 1). Monthly mean surface air temperature and precipitation (MERRA-2 reanalysis data)  
110 over the selected glaciers were analyzed and compared for the western and central Himalayan glaciers from April  
111 2015 to October 2017 (Table 2). Yala Glacier is a plateau-shaped glacier that has an elevation range between 5160  
112 and 5750 m a.s.l. The length of the Yala glacier is 1.5 km facing the northwest. The glacier is located away from the  
113 residential area and is mostly covered by firm/snow especially during the winter season. Details about the  
114 metrological condition at the Yala glacier are available in Mukesh et al., (2019) and Gul et al., (2021). Thana glacier  
115 is a gentle slope glacier with slight debris cover and an elevation range between 5250 and 5700 m a.s.l. The length  
116 of the glacier is about 5 km, facing the southwest. The Thana glacier is mostly covered by fresh snow especially  
117 during the winter season. The Sachin glacier has a gentle slope with dense debris cover in its ablation area with an  
118 altitude range from 3105 to 4976 m a.s.l. The length of the Sachin glacier is around 8 km facing northeast. In  
119 general, the Sachin, glacier is low elevated and relatively debris-covered glaciers as compared to central Himalayan  
120 glaciers (Yala and Thana). Precipitation in central Himalayan glaciers (Yala and Thana) was higher than that of the  
121 western Himalayan glacier (Sachin) especially from April to October each year (Table 2). Surface air temperature  
122 over the Yala and Sachin glacier was higher than that of the Thana glacier. The geographical location of the selected



123 glaciers and snow sampling locations are shown in Fig. 1. Besides the difference in altitude, latitude, and  
124 meteorology of the selected glaciers in the central and western Himalayas, there is also a difference in the surface  
125 condition shown in supplementary Fig. S1.

126

### 127 **3 Methodologies**

128

#### 129 **3.1 Snow sampling and analysis**

130 Snow samples were collected from the central and western Himalayan glaciers during May, and September 2016.  
131 Samples were taken from the surface of the selected glaciers; however, few snow samples were also collected from  
132 the surrounding nearby areas of the Yala and Sachin glaciers. The snow density was measured with a small density  
133 kit. The snow grain size was measured through a hand lens (25×) with an accuracy of 0.02mm. A detailed  
134 description of the sampling procedure is described in Gul et al., 2021. Quartz filters were used to measure the mass  
135 concentration of BC, OC, and dust in the collected samples. BC and OC present in snow samples were analyzed by a  
136 filter-based thermal-optical analysis method using DRI® Model 2005 (Chow et al., 1993). Filters were analyzed at  
137 the State Key Laboratory of Cryosphere Science, Northwest Institute of Eco-Environment and Resources, Chinese  
138 Academy of Sciences. Before starting the analysis, a piece of the sampled filters was put in an oven for a few  
139 minutes to eliminate the water vapor content and volatile organic compounds. Further detailed information on the  
140 instrument and analysis method can be referred to in earlier studies (Gul et al., 2018, 2021).

141

#### 142 **3.2 Estimation of snow albedo reduction and radiative forcing**

143 The online snow simulation model SNICAR (Flanner et al., 2007, <http://snow.engin.umich.edu/>) was used to  
144 estimate snow albedo calculation for the collected samples. The model has been used by multiple studies in the past  
145 (e.g., Li et al., 2017; Gul et al., 2018; Zhang et al., 2018 ). Albedo was simulated based on an hourly SZA at the  
146 sampling site with an averaged mass concentration of BC, dust, and other input parameters such as snow grain size,  
147 snow density, and snow depth from measurements. We computed broadband snow albedo for direct solar incident  
148 radiation under the mid-latitude winter clear sky condition, (Supplementary Table S1). Depending on geographical  
149 location, 10 to 15 SZAs were used (between 0° and 90°) during instantaneous daytime albedo simulation. Albedo  
150 was simulated in four categories: 1- broadband albedo with BC and dust in snow, 2- broadband albedo with BC in  
151 snow only, 3- broadband albedo with dust in snow only, and 4- broadband albedo with the absence of BC and dust  
152 which was considered as a reference albedo. Radiative implications caused by snow darkening due to BC and dust  
153 deposition were investigated using the albedo reduction and the radiative transfer model Santa Barbara DISORT  
154 Atmospheric Radiative Transfer (SBDART) (Ricchiuzzi et al., 1998). To evaluate the amount of additional solar  
155 radiations absorbed by the snow in the presence of BC and dust, we estimated the mean solar irradiance and its  
156 characteristics via SBDART, which has been used in the past (Yang et al., 2015). According to the location of the  
157 sampling site, the characteristics of the atmospheric profiles such as water vapor, aerosols, ozone, etc. were set in the  
158 model. RF-based on measured BC and dust concentration in our samples were estimated using the following  
159 equation.



160  $RF_x = R_{in-short} * \Delta \alpha_x$  ----- (1)

161 where,  $R_{in-short}$  denotes incident short-wave solar radiation for selected SZA and  $\Delta \alpha_x$  denotes the reduction in albedo  
162 due to BC, dust, or both, as simulated by the SNICAR model.

163

### 164 **3.3 Potential source region of pollutants**

165 Glaciers of the Himalaya Karakoram and Hindukush (HKH) region are located at high altitudes as compared to the  
166 sources of the major pollutants. LAPs including BC and dust can transport from urban areas towards glaciated areas  
167 (e.g., Yasunari et al., 2009; Kang et al., 2019). Multiple approaches, including climate circulation modeling,  
168 combinations of bottom-up inventories, and back air trajectories have been used in the past to determine the possible  
169 source regions of pollution in the HKH region. To identify the potential source region of pollution for the central  
170 and western Himalayan glaciers, the weather research and forecasting (WRF) model coupled with chemistry (WRF-  
171 Chem version 3.9.1.1) (Grell et al., 2005) tagged-tracer simulations for the selected sites.

172

173 WRF-Chem simulations were used to estimate BC mass concentration in surface snow and deposition of BC  
174 particles on three selected glaciers (Yala, Thana, and Sachin). We archived the hourly model results for  
175 instantaneous BC deposition and concentration in snow. The horizontal grid spacing of the model was 20 km x 20  
176 km with 35 vertical levels stretching from the surface up to 50 hPa (~20 km). The updated Model for OZone And  
177 Related chemical Tracers (MOZART) was applied for the gas phase chemistry (Knote et al., 2014) while aerosols in  
178 the WRF-Chem were simulated via the Model for Simulating Aerosol Interactions and Chemistry (MOSAIC)  
179 (Zaveri et al., 2008). We use the Global Data Assimilation System (GDAS) from the National Center for  
180 Environmental Prediction (NCEP) for the meteorological initial and boundary conditions. We used the Fire  
181 Inventory from NCAR (FINN), the EDGAR-HTAP, and MEGAN (Model of Emissions of Gases and Aerosols from  
182 Nature) for biomass burning emissions, anthropogenic emissions, and for online biogenic emissions, respectively.  
183 For chemical boundary conditions, we used the NCAR global CAM-Chem simulation dataset  
184 (<https://rda.ucar.edu/datasets/ds313.7/>). Key meteorological variables such as winds, temperature, and water vapor  
185 above the planetary boundary layer (PBL) were nudged every 6 hours towards the NCEP GDAS reanalysis fields to  
186 reduce temporal error growth in meteorological variables. We used the Community Land Model (CLM) scheme for  
187 the land component in WRF-Chem. The CLM model can simulate BC concentration in snowpack and its effects on  
188 snow albedo (Flanner et al., 2007). We used online coupled BC deposition fluxes from the atmosphere component  
189 of WRF-Chem with the CLM model following Zhao et al. (2014). We also implemented a tagged-tracer method  
190 (Kumar et al., 2015) to track anthropogenic BC emissions from 10 different Asian countries surrounding the TP  
191 areas, as well as BC emissions from Asian biomass burning and the domain boundary (i.e., areas outside Asia). The  
192 tracked 10 anthropogenic emission source regions include China, India, Nepal, Pakistan, Afghanistan, Bhutan,  
193 Bangladesh, Myanmar, Southeast Asia, and the rest of Asia. The aim of the model simulation was to estimate the  
194 BC mass concentration in surface snow, deposition of BC particles, and the source contribution to BC deposition on  
195 snow.

196



## 197 4. Results and discussions

### 198 4.1 Concentrations of light-absorbing particles in surface snow

199 The average mass concentration of LAPs in surface snow of the Yala glacier was  $357.93 \text{ ng g}^{-1}$  for BC,  $903.86 \text{ ng g}^{-1}$   
200 for OC, and  $21.95 \text{ } \mu\text{g g}^{-1}$  for dust in spring (May) and was relatively lower concentrations of  $68.97 \text{ ng g}^{-1}$  for BC,  
201  $177.50 \text{ ng g}^{-1}$  for OC and  $4.3 \text{ ng g}^{-1}$  for dust during autumn (September). These mass concentrations of BC and OC  
202 in surface snow were comparable to the study result conducted on the Yala glacier in May 2017 (Gul et al., 2021).  
203 High LAP concentration in the pre-monsoon is due to a seasonally high Indian subcontinent emission (Kang et al.,  
204 2019; Gul et al., 2021); Lau et al., (2010) also confirmed that aerosols from biofuel and biomass burning rapidly  
205 build up over Indo-Gangetic Plains (IGP) and East Asia during pre-monsoon season and move towards the study  
206 site. The average surface concentrations of BC, OC, and dust in the Thana glacier samples during the autumn season  
207 were  $39.39 \text{ ng g}^{-1}$ ,  $115 \text{ ng g}^{-1}$  and  $34.63 \text{ } \mu\text{g g}^{-1}$ , respectively. Possible reasons for the lowest concentration at the  
208 Thana glacier may be due to the relatively high elevation of sampling location and relatively fresh snow. A strong  
209 effect of LAPs (BC and dust) has been observed at lower elevations in comparison to higher elevations (Li et al.,  
210 2017). The average concentration of BC, OC, and dust measured in the selected western Himalayan glacier (Sachin)  
211 during May were  $2381.39 \text{ ng g}^{-1}$ ,  $3896 \text{ ng g}^{-1}$  and  $101 \text{ } \mu\text{g g}^{-1}$ , respectively, and were relatively higher during October  
212 with values of  $5314 \text{ ng g}^{-1}$  for BC, and  $546 \text{ } \mu\text{g g}^{-1}$  for dust (Gul et al., 2018). The observed average mass  
213 concentrations in the western Himalayas were higher than those in the central Himalayas. The BC mass  
214 concentration difference might be due to the difference in snow type, precipitation rate, and local emission, the  
215 elevation of sampling sites, meteorology, and BC deposition over the glacier surfaces. Post dry deposition of LAPs  
216 over the surface of the snow was an important factor. Snow samples collected from the western side of the  
217 Himalayas were aged as compared to the central side; post-deposition ion (or enrichment) of LAPs over the snow  
218 surface increased the concentration in the snow (Kang et al., 2019). The majority of the samples from the western  
219 Himalayan side were from ablation zones of the glacier, where concentrations of LAPs are higher as compared to  
220 the accumulation zone of the glacier. Li et al., (2017) showed a strong negative relationship between the elevation of  
221 glacier sampling locations and the concentration of LAPs. Therefore strong melting of surface snow and ice in the  
222 glacier ablation zone could lead to BC enrichment which causes high BC concentrations (Li et al., 2017). In the  
223 case of western Himalayan glaciers sites, snow samples were collected long after the snowfall and the concentration  
224 of pollutants would also have increased in the surface snow due to dry deposition. The surface concentrations of the  
225 individual samples collected from the Yala, Thana, and Sachin glaciers during May and September 2016 are shown  
226 in Fig. 2, and Table S2. BC and OC concentration on our selected glaciers with a comparison to other glaciers of TP  
227 and the surrounding region are shown in Fig. 4 and Table S3. It was observed that the concentration of BC, OC, and  
228 dust in the central Himalayan glaciers (Yala and Thana) were comparable to other reported results. In the past,  
229 similarly high concentrations were reported in the region (Xu et al., 2012) such as Tien Shan Mountains (Li et al.,  
230 2016), Northeast of the TP (Wang et al., 2016), Northern China (Zhang et al., 2016) Southeastern TP, western Tien  
231 Shan and Central Asia (Zhang et al., 2017).

232



233 The yellow boxes of Fig. 2 show the WRF-Chem modeled BC concentrations in surface snow at the three  
234 measurement glacier sites during the measurement periods. Compared to the observations red boxes in Fig. 2, model  
235 results reasonably capture the spatial and seasonal patterns and variables of the observed BC in the snow with a  
236 relatively smaller magnitude. The modeled variation at the Sachin site during the October sampling periods is much  
237 larger than the observations (Gul et al., 2008). The discrepancies between model results and observations are due to  
238 model uncertainties from (1) the relatively coarse grid spacing that may not capture the transport over the complex  
239 TP terrain, (2) the underestimated anthropogenic emissions that are not representative for the measurement periods,  
240 and (3) deficiencies in model physical parameterizations that affects BC transport and deposition. We also note that  
241 the observed variation at each site shown in Fig. 2 includes both the temporal and subgrid variabilities derived from  
242 multiple sampling locations surrounding each site (Fig. 1). In contrast, all the measurement locations at each  
243 particular glacier site are located within a single model grid. As a result, the model is unable to resolve this subgrid  
244 information and hence only includes the temporal variability for each selected site.

245

#### 246 **4.2 Surface snow albedo and radiative forcing**

247 The minimum daytimes absolute albedo reduction due to combined BC and dust, BC only and dust only were in the  
248 range (1.03-13.44%), (0.48-12.42%) and (0.12-2.12%), respectively. The maximum daytime albedo reduction due to  
249 combined BC and dust, BC only and dust only was in the range (1.98-24.97%), (1.05-24%), and (0.25-4.8%)  
250 respectively. The lowest and highest contributions in albedo reduction were observed in the central Himalayas  
251 (September) and the western Himalayas (May) respectively. Snow albedo reduction (%) derived from samples  
252 collected from the Yala glacier (during May 2016) and the Thana glacier (during September 2016) were in the range  
253 of (0.13-3.82%) and (0.90-1.99%), respectively. A significant difference in daytime albedo reduction between the  
254 western and central Himalayas was mainly due to the difference in mass concentrations of pollutants and snow age.  
255 The pollutant concentrations in the western Himalayan samples (Sachin glacier) were higher, resulting in higher  
256 albedo reduction as compared to the central Himalayan (Yala and Thana glaciers) samples. The average elevation  
257 difference between central and western sampling sites was greater than 1000 meters, where a high concentration of  
258 pollution is expected at the low elevated glacier of the western side as compared to the central side of the Himalaya.  
259 Snow samples collected on the central side of the Himalayas (Yala glacier) were much fresher as compared to the  
260 samples collected from the western side (Sachin glacier). Dust and other pollutants were visible over the surface of  
261 the Sachin glacier (Fig. S1). Aged snow had increased density, enlarged grain size, and increased concentration of  
262 BC and dust particles due to dry deposition on the snow surface. In the case of all sampling sites impact of BC on  
263 snow albedo reduction was greater than the impact of dust except the Thana glacier where the impact of dust was  
264 higher than that of BC (Fig. 4a). This may be due to a different dust type in Thana samples. Daytime snow albedo  
265 reductions (%) due to BC only, dust only, and both BC and dust are given in Fig. 4a.

266

267 The daytime instantaneous RF ( $W m^{-2}$ ) ranged from (0.076 to 39.65) for the Yala glacier during May 2016, 0.006 to  
268 18.26 for the Yala glacier during September 2016, 0.0 to 11.48 for the Thana glacier during September 2016, and  
269 0.03 to 96.48 for the Sachin glacier during May 2016. RF for the western Himalayas (Sachin glacier) was quite high





270 as compared to the central Himalayan glaciers (Yala and Thana glaciers). The radiative effect on the Sachin glacier  
271 was much more than that of other selected glaciers mainly due to low albedo and increased temperature. Zhang et al.  
272 (2017) reported that a reduction in albedo by 9 to 64 % can increase the instantaneous RF by as much as 24.05–  
273 323.18 W m<sup>-2</sup>. In the case of all sampling sites impact of BC on RF was greater than the impact of dust except the  
274 Thana glacier where the impact of dust was higher than that of BC (Fig. 4b). Therefore, BC can be a major  
275 responsible pollutant in the snow to reduce albedo and increase warming in the selected glaciers. BC was the  
276 dominant factor in snow melting in the Yala and Sachin glaciers; however, dust was the dominant factor in Thana  
277 glacier samples. According to (Kaspari et al., 2014), RF caused by mineral dust was greater than that of dust. The  
278 BC and dust had low importance for RF in fresh snow (central Himalaya - Thana glacier) as compared to aged snow  
279 (western Himalaya - Sachin glacier). In the northern TP, BC played important role in RF (Li et al., 2016a), while in  
280 the central TP and Himalayas dust was more important than BC (Kaspari et al., 2014). The average instantaneous  
281 RF caused by the combined contribution of BC and dust (BC + dust), only BC, and only dust is shown in Fig. 4b as  
282 a function of surface snow types. Variation in the RF and albedo change for a particular pollutant type was due to  
283 variation in SZA.

284

## 285 **5 Potential source regions of pollutants**

286 Figure 5 shows the contributions of different BC emission sources to the BC in snow from WRF-Chem tagged-  
287 tracer simulations. For the Yala site, it is dominated (>50%) by anthropogenic emissions from India and Nepal for  
288 both May and October, while the biomass burning contribution (>20%) increases largely in May primarily due to the  
289 spring burning activities in northern India (Kumar et al., 2011). In September, China's contribution also increases to  
290 >20% at Yala. For the Thana site, it is dominated (>60%) by anthropogenic emissions from China and India in  
291 September, while anthropogenic emissions from Bhutan and Myanmar also contribute about 10%, respectively. The  
292 Sachin site is predominantly affected by anthropogenic emissions from India and Pakistan (total contribution  
293 >80%), while the spring biomass burning only contributes to ~10% in May. Overall, the source contributions show  
294 large variation depending on the site locations and sampling seasons, but with a consistent India contribution of 20-  
295 40% across all the sites and seasons.

296

## 297 **6 Discussion on uncertainty in measurements, albedo, and potential source identification of pollutants**

298 The possible uncertainties in the present research were related to measurements, sampling, analysis, albedo, and RF  
299 estimation. A sampling at remote rural sites, sample preservation, filtration, and transport can modify the results if  
300 proper standard protocols were not followed. During laboratory analysis via thermal optical techniques, several  
301 uncertainties may be related to separating OC from BC in the sample (Gul et al., 2021). The level of generated  
302 uncertainty depended on temperature protocol, sample type (residential cookstoves, diesel exhaust, rural aerosols,  
303 and urban aerosols), the amount of dust loading on the filter, and the analysis method. The overall accuracy in the  
304 measurement of OC, BC, and total carbon concentrations was estimated considering the mass contributions from  
305 field blanks and the analytical accuracy of concentration measurements. The uncertainty of the OC and BC mass  
306 concentrations was extracted through the standard deviation of the field blanks (li et al., 2021). OC in snow can



307 produce minor warming (Yasunari et al., 2015), but in this research albedo reduction from OC was not quantified. In  
308 albedo simulation and RF estimations, snow grain size and texture can produce large uncertainty. We  
309 measured/considered the physical grain size in this research which is not the same as the effects than optical grain  
310 size. Optical grain size defines the amount of solar radiation absorbed/scattered by the snow. We assumed a  
311 spherical shape for the snow grains which may affect the results because the albedo of non-spherical grains is higher  
312 than the albedo of spherical grains (Dang et al., 2016; He et al., 2018). The contribution of pollutants generated from  
313 local sources can be important (e.g., Li et al., 2021), which however was not included in the global emission  
314 inventories; we were unable to capture emissions at the local scale. Therefore contributions of local sources may be  
315 underestimated by coarse-resolution models. High-resolution models and emission inventories at the local scale are  
316 required to capture local emissions.

317

## 318 **7 Conclusions**

319 The average mass concentration of LAPs in the samples collected from the Sachin, Yala, and Thana glaciers were in  
320 the range (835.324 ng g<sup>-1</sup> to 3545.35 ng g<sup>-1</sup> for BC and 35.24 µg g<sup>-1</sup> to 253.52 µg g<sup>-1</sup> for Dust), (23.16 ng g<sup>-1</sup> to  
321 2529 ng g<sup>-1</sup> for BC and 1.5 µg g<sup>-1</sup> to 196.5 µg g<sup>-1</sup> for Dust), and (21 ng g<sup>-1</sup> to 127 ng g<sup>-1</sup> for BC and 1.5 µg g<sup>-1</sup> to 67  
322 µg g<sup>-1</sup> for Dust) respectively. Overall the concentrations of BC and dust were varied from 21 ng g<sup>-1</sup> and 1.5 µg g<sup>-1</sup> in  
323 fresh snow to 3545 ng g<sup>-1</sup> and 253 µg g<sup>-1</sup> in the aged snow, respectively. Mass concentrations of BC, OC, and dust in  
324 the samples collected from the western Himalayas was much higher than the average concentration in the central  
325 Himalayas mainly due to difference in snow age, elevation, and meteorology. The accumulation area of glaciers  
326 (e.g. ice cores and snow pits), where enrichment influences are less marked and measured values are likely to be  
327 lower, and high elevation areas, where deposition of pollutants is expected to be lower. Pollutant concentrations  
328 were likely underestimated in the earlier studies, particularly when there was strong surface melting. Dust and other  
329 pollutants were visible on aged snow surfaces in the western Himalaya, indicating considerable enrichment during  
330 snow aging. WRF-Chem modeled BC concentrations in surface snow were almost similar to the observed BC in the  
331 snow with a relatively smaller magnitude.

332

333 Based on observed pollutants, snow albedo reduction (%) in the central Himalayas was in the range of (0.48-3.6%  
334 for BC) and (0.13-1.99% for Dust), much lower than that of the western Himalayas. BC was the major component  
335 responsible for the albedo reduction, and the dust had little effect except in the Thana glacier. In case the of the  
336 Thana glacier, the impact of dust was higher than that of BC. The daytime instantaneous radiative forcing (W m<sup>-2</sup>)  
337 ranged from 0.076 to 39.65 (Yala glacier during May 2016), 0.006 to 18.26 (Yala glacier during September 2016),  
338 0.0 to 11.48 (Thana glacier during September 2016), 0.03 to 96.48 (Sachin glacier during May 2016). The average  
339 albedo reduction due to the combined effect of dust and BC at the western Himalayan side (Sachin glacier) was  
340 0.372 which was ~15 times higher than that of the central Himalayan side (Yala glacier). Similarly, the radiative  
341 forcing in the western Himalayas was ~6 times higher than that of the central Himalayan side. Observation showed  
342 that the potential source regions of pollutants for the western and central Himalayas were different. Western  
343 Himalayan glaciers were mostly affected by long-range transport via the westerlies; however central Himalayan



344 glaciers were affected by relatively local winds from Nepal, Bhutan, India, and China. For the western Himalayan  
345 glaciers, the emissions from central Asian and South Asian countries (Particularly Pakistan and India) are more  
346 important source regions.

347

#### 348 **Acknowledgment**

349 This study was supported by the National Natural Science Foundation of China (41630754), the Chinese Academy  
350 of Sciences (XDA20040501, QYZDJ-SSW-DQC039), and the State Key Laboratory of Cryosphere Science  
351 (SKLCS-ZZ-2021). This study was also partially supported by the core funds of ICIMOD contributed by the  
352 governments Afghanistan, Australia, Austria, Bangladesh, Bhutan, China, India, Myanmar, Nepal, Norway,  
353 Pakistan, Sweden, and Switzerland. We thank Arnico Panday, Lubna ayaz and Aditi Mukherji for their useful  
354 comments and guidance. We are also grateful to the staff of the National Centre for Hydrology and Meteorology in  
355 Bhutan for organizing the Thana Glacier expedition in 2016. We would like to acknowledge high-performance  
356 computing support from Cheyenne provided by NCAR's Computational and Information Systems Laboratory,  
357 sponsored by the National Science Foundation. NCAR is operated by the University Corporation for Atmospheric  
358 Research under the sponsorship of the National Science Foundation.

359

#### 360 **References**

- 361 Bolch, T., Kulkarni, A., Kääb, A., Huggel, C., Paul, F., Cogley, J. G., Frey, H., Kargel, J. S., Fujita, K., Scheel, M.,  
362 Bajracharya, S., and Stoffel, M.: The State and Fate of Himalayan Glaciers, *Science*, 336, 310–314, 2012.
- 363 Bond, T. C., Doherty, S. J., Fahey, D. W., Forster, P. M., Bernsten, T., DeAngelo, B. J., Flanner, M. G., Ghan, S.,  
364 Kärcher, B., Koch, D., Kinne, S., Kondo, Y., Quinn, P. K., Sarofim, M. C., Schultz, M. G., Schulz, M.,  
365 Venkataraman, C., Zhang, H., Zhang, S., Bellouin, N., Guttikunda, S. K., Hopke, P. K., Jacobson, M. Z., Kaiser,  
366 J. W., Klimont, Z., Lohmann, U., Schwarz, J. P., Shindell, D., Storelvmo, T., Warren, S. G., and Zender, C. S.:  
367 Bounding the role of black carbon in the climate system: A scientific assessment, *J. Geophys. Res.-Atmos.*, 118,  
368 5380–5552, doi:10.1002/jgrd.50171, 2013.
- 369 Chow, J. C., Watson, J. G., Pritchett, L. C., Pierson, W. R., Frazier, C. A., and Purcell, R. G.: The DRI  
370 thermal/optical reflectance carbon analysis system: description, evaluation, and applications in US air quality  
371 studies, *Atmos. Environ. A-Gen.*, 27, 1185–1201, 1993.
- 372 Dang, C., Zender, C. S., and Flanner, M. G. (2019), Intercomparison and improvement of twostream shortwave  
373 radiative transfer schemes in Earth system models for a unified treatment of cryospheric surfaces, *The*  
374 *Cryosphere*, 13, 2325–2343, doi:10.5194/tc-13-2325-2019, 2019.
- 375 Dang, C., Fu, Q., and Warren, S. G.: Effect of snow grain shape on snow albedo, *J. Atmos. Sci.*, 73, 3573–  
376 3583, <https://doi.org/10.1175/JAS-D-15-0276.1>, 2016.
- 377 Flanner, M. G. and Zender, C. S.: Linking snowpack microphysics and albedo evolution, *J. Geophys. Res. Atmos.*,  
378 111(12), 1–12, doi:10.1029/2005JD006834, 2006.
- 379 Flanner, M. G., Zender, C. S., Randerson, J. T. and Rasch, P. J.: Present-day climate forcing and response from black



- 380 carbon in snow, *J. Geophys. Res. Atmos.*, 112(11), 1–17, doi:10.1029/2006JD008003, 2007.
- 381 Flanner, M. G., Zender, C. S., Hess, P. G., Mahowald, N. M., Painter, T. H., Ramanathan, V. and Rasch, P. J.:  
382 Springtime warming and reduced snow cover from carbonaceous particles, *Atmos. Chem. Phys. Discuss.*, 8(6),  
383 19819–19859, doi:10.5194/acpd-8-19819-2008, 2009.
- 384 Grell, G. A., Peckham, S. E., Schmitz, R., McKeen, S. A., Frost, G., Skamarock, W. C., and Eder, B.: Fully coupled  
385 “online” chemistry within the WRF model, *Atmos. Environ.*, 39, 6957–6975, 2005.
- 386 Gul, C., Puppala, S.P., Kang, S., Adhikary, B., Zhang, Y., Ali, S., Li, Y., Li, X., 2018. Concentrations and source  
387 regions of light-absorbing particles in snow/ice in northern Pakistan and their impact on snow albedo. *Atmos.*  
388 *Chem. Phys.* 18, 4981–5000. <https://doi.org/10.5194/acp-18-4981-2018>
- 389 Gul, C., Mahapatra, P.S., Kang, S., Singh, P.K., Wu, X., He, C., Kumar, R., Rai, M., Xu, Y., Puppala, S.P., Black  
390 carbon concentration in the central Himalayas: impact on glacier melt and potential source contribution,  
391 *Environmental Pollution*, <https://doi.org/10.1016/j.envpol.2021.116544>.
- 392 Hansen, J. and Nazarenko, L.: Soot climate forcing via snow and ice albedos, *Proc. Natl. Acad. Sci. U. S. A.*, 101(2),  
393 423–428, doi:10.1073/pnas.2237157100, 2004.
- 394 Hansen, J., Sato, M. & Ruedy, R.: Radiative forcing and climate response, *J. Geophys. Res.* 102, 6831–6864,  
395 doi.org/10.1029/96JD03436, 1997
- 396 He, C., Flanner, M. G., Chen, F., Barlage, M., Liou, K.-N., Kang, S., Ming, J., and Qian, Y.: Black carbon-induced  
397 snow albedo reduction over the Tibetan Plateau: uncertainties from snow grain shape and aerosol–snow mixing  
398 state based on an updated SNICAR model, *Atmos. Chem. Phys.*, 18, 11507–11527, [https://doi.org/10.5194/acp-](https://doi.org/10.5194/acp-18-11507-2018)  
399 [18-11507-2018](https://doi.org/10.5194/acp-18-11507-2018), 2018
- 400 He, C., & Flanner, M. (2020). Snow Albedo and Radiative Transfer: Theory, Modeling, and  
401 Parameterization. Kokhanovsky A, editor, 67-133.
- 402 He, C., Takano, Y., Liou, K. N., Yang, P., Li, Q., & Chen, F. (2017). Impact of snow grain shape and black carbon–  
403 snow internal mixing on snow optical properties: Parameterizations for climate models. *Journal of*  
404 *Climate*, 30(24), 10019-10036. doi:10.1175/JCLI-D-17-0300.1
- 405 Hock R.: Glacier melt: a review of processes and their modelling. *Progr. Phys. Geogr.*, 29(3), 362–391, doi:  
406 10.1191/0309133305pp453ra, 2005.
- 407 Hock, R., G. Rasul, C. Adler, B. Cáceres, S. Gruber, Y. Hirabayashi, M. Jackson, A. Käab, S. Kang, S. Kutuzov, Al.  
408 Milner, U. Molau, S. Morin, B. Orlove, and H. Steltzer, 2019: High Mountain Areas. In: *IPCC Special Report on*  
409 *the Ocean and Cryosphere in a Changing Climate* [H.-O. Pörtner, D.C. Roberts, V. Masson-Delmotte, P. Zhai,  
410 M. Tignor, E. Poloczanska, K. Mintenbeck, A. Alegria, M. Nicolai, A. Okem, J. Petzold, B. Rama, N.M. Weyer  
411 (eds.)]. In press.
- 412 Immerzeel, W. W., van Beek, L. P. H. and Bierkens, M. F. P.: Climate change will affect the Asian water towers.,  
413 *Science*, 328(5984), 1382–5, doi:10.1126/science.1183188, 2010.
- 414 Ji Z., S. Kang, Z. Cong, Q. Zhang, T. Yao. 2015. Simulation of carbonaceous aerosols over the Third Pole and  
415 adjacent regions: distribution, transportation, deposition, and climatic effects. *Climate Dynamics*, 45(9-10):  
416 2831-2846. <https://doi.org/10.1007/s00382-015-2509-1>.



- 417 Kang S., Y. Zhang, Y. Qian, H. Wang. 2020. A review of black carbon in snow and ice and its impacts on  
418 cryospheric change. *Earth-Science Reviews*, 210, 103346. <https://doi.org/10.1016/j.earscirev.2020.103346>.
- 419 Kang S., Q. Zhang, Y. Qian, Z. Ji, C. Li, Z. Cong, Y. Zhang, J. Guo, W. Du, J. Huang, Q. You, A. K. Panday, M.  
420 Rupakheti, D. Chen, Örjan Gustafsson, M. H. Thiemens, D. Qin. 2019. Linking Atmospheric Pollution to  
421 Cryospheric Change in the Third Pole Region: Current Progresses and Future Prospects. *National Science*  
422 *Review*, 6(4): 796-809. <https://doi.org/10.1093/nsr/nwz031>.
- 423 Kang S., X. Wei, Q. You, Wolfgang-Albert Flügel, Nick Pepin, T. Yao. 2010. Review of climate and cryospheric  
424 change in the Tibetan Plateau. *Environmental Research Letter*, 5(2010) 015101 (8pp).  
425 <https://doi.org/10.1088/1748-9326/5/1/015101>.
- 426 Kaspari, S., Painter, T. H., Gysel, M., Skiles, S. M. and Schwikowski, M.: Seasonal and elevational variations of  
427 black carbon and dust in snow and ice in the Solu-Khumbu, Nepal and estimated radiative forcings, *Atmos.*  
428 *Chem. Phys.*, 14(15), 8089–8103, doi:10.5194/acp-14-8089-2014, 2014.
- 429 Knote, C., Hodzic, A., Jimenez, J. L., Volkamer, R., Orlando, J. J., Baidar, S., Brioude, J., Fast, J., Gentner, D. R.,  
430 Goldstein, A. H., Hayes, P. L., Knighton, W. B., Oetjen, H., Setyan, A., Stark, H., Thalman, R., Tyndall, G.,  
431 Washenfelder, R., Waxman, E., and Zhang, Q.: Simulation of semi-explicit mechanisms of SOA formation from  
432 glyoxal in aerosol in a 3-D model, *Atmos. Chem. Phys.*, 14, 6213–6239, doi:10.5194/acp-14-6213-2014, 2014.
- 433 Kumar, R., Barth, M. C., Nair, V. S., Pfister, G. G., Suresh Babu, S., Satheesh, S. K., Krishna Moorthy, K.,  
434 Carmichael, G. R., Lu, Z., and Streets, D. G.: Sources of black carbon aerosols in South Asia and surrounding  
435 regions during the Integrated Campaign for Aerosols, Gases and Radiation Budget (ICARB), *Atmos. Chem.*  
436 *Phys.*, 15, 5415-5428, <https://doi.org/10.5194/acp-15-5415-2015>, 2015.
- 437 Kumar, R., Naja, M., Satheesh, S. K., Ojha, N., Joshi, H., Sarangi, T., Pant, P., Dumka, U. C., Hegde, P.,  
438 and Venkataramani, S. (2011), Influences of the springtime northern Indian biomass burning over the central  
439 Himalayas, *J. Geophys. Res.*, 116, D19302, doi:10.1029/2010JD015509.
- 440 Lau, K. M., Kim, M. K., and Kim, K. M.: Enhanced surface warming and snow melt in the Himalayas and Tibetan  
441 Plateau induced by the EHP effect, *Environ. Res. Lett.*, 5, 025204, doi:10.1088/1748-9326/5/2/025204, 2010.
- 442 Li, C., Yan, F., Kang, S., Yan, C., Hu, Z., Chen, P., ... & Stubbins, A. (2021). Carbonaceous matter in the atmosphere  
443 and glaciers of the Himalayas and the Tibetan plateau: An investigative review. *Environment International*, 146,  
444 106281
- 445 Li, X., Kang, S., He, X., Qu, B., Tripathee, L., Jing, Z., Paudyal, R., Li, Y., Zhang, Y., Yan, F., Li, G. and Li, C.:  
446 Light-absorbing impurities accelerate glacier melt in the Central Tibetan Plateau, *Sci. Total Environ.*,  
447 doi:10.1016/j.scitotenv.2017.02.169, 2017.
- 448 Li, Yang, S. Kang, Xuelei Zhang, Jizu Chen, Julia Schmale, Xiaofei Li, Yulan Zhang, Hewen Niu, Zhongqin Li,  
449 Xiang Qin, Xiaobo He, Wei Yang, Guoshuai Zhang, Shijin Wang, Lili Shao, Lide Tian. 2021. Black carbon and  
450 dust in the Third Pole glaciers: Revaluated concentrations, mass absorption cross-sections and contributions to  
451 glacier ablation. *Science of the Total Environment*, 789: 147746. <https://doi.org/10.1016/j.scitotenv.2021.147746>.
- 452 Marcovecchio, A., Behrangi, A., Dong, X., Xi, B., Huang, Y. Precipitation Influence on and Response to Early and  
453 Late Arctic Sea Ice Melt Onset During Melt Season. *International Journal of Climatology*



- 454 Mayer C, Lambrecht A, Belo` M, Smiraglia C and Diolaiuti G.: Glaciological characteristics of the ablation zone of  
455 Baltoro glacier, Karakoram, Pakistan. *Ann. Glaciol.*, 43, 123–131, doi: 10.3189/172756406781812087, 2006
- 456 Niu, H., Kang, S., Wang, H., Du, J., Pu, T., Zhang, G., Lu, X., Yan, X., Wang, S., Shi, X., 2020. Light-absorbing  
457 impurities accelerating glacial melting in southeastern Tibetan Plateau. *Environ. Poll.* 257, 113541.  
458 <https://doi.org/10.1016/j.envpol.2019.113541>.
- 459 Rai M., Mahapatra P.S., Gul C. et al., Aerosol Radiative Forcing Estimation over a Remote High-altitude Location  
460 (~4900 masl) near Yala Glacier, Nepal, *Journal of Aerosol and Air Quality Research*, 19: 1872–1891, doi:  
461 10.4209/aaqr.2018.09.0342, 2019
- 462 Pepin N C and Lundquist J D 2008 Temperature trends at high elevations: patterns across the globe *Geophys. Res.*  
463 *Lett.* 35 L14701
- 464 Qian, Y., Flanner, M. G., Leung, L. R. and Wang, W. 2011. Sensitivity studies on the impacts of Tibetan Plateau  
465 snowpack pollution on the Asian hydrological cycle and monsoon climate. *Atmos. Chem. Phys.* 11, 1929–1948.
- 466 Qu, B., Ming, J., Kang, S. C., Zhang, G. S., Li, Y. W., Li, C. D., Zhao, S. Y., Ji, Z. M. and Cao, J. J.: The decreasing  
467 albedo of the Zhadang glacier on western Nyainqentanglha and the role of light-absorbing impurities, *Atmos.*  
468 *Chem. Phys.*, 14(20), 11117–11128, doi:10.5194/acp-14-11117-2014, 2014.
- 469 Quinn, P. K., Bates, T. S., Baum, E., Doubleday, N., Fiore, A. M., Flanner, M., Fridlind, A., Garrett, T. J., Koch, D.,  
470 Menon, S., Shindell, D., Stohl, A., and Warren, S. G.: Short-lived pollutants in the Arctic: their climate impact  
471 and possible mitigation strategies, *Atmos. Chem. Phys.*, 8, 1723–1735, doi:10.5194/acp-8-1723-2008, 2008.
- 472 Ramanathan, V., and Carmichael, G.: Global and regional cli- mate changes due to black carbon, *Nat. Geosci.*, 1,  
473 221–227, doi:10.1038/Ngeo156, 2008.
- 474 Ricchiuzzi, P., Yang, S. R., Gautier, C., and Soble, D.: SBDART: A research and teaching software tool for plane-  
475 parallel radiative transfer in the Earth’s atmosphere, *B. Am. Meteorol. Soc.*, 79, 2101–2114, 1998.
- 476 Schmale, J., Flanner, M., Kang, S., Sprenger, M., Zhang, Q., Guo, J., Li, Y., Schwikowski, M., Farinotti, D., 2017.  
477 Modulation of snow reflectance and snowmelt from Central Asian glaciers by anthropogenic black carbon. *Sci.*  
478 *Rep.* 7, 40501. <https://doi.org/10.1038/srep40501>.
- 479 Vaux, H. J., Jr., Balk, D., Cook, E. R., Gleick, P., Lau, W. K.-M. et al.: *Himalayan Glaciers: Climate Change, Water*  
480 *Resources, and Water Security*. National Academies Press, Washington, DC, 2012.
- 481 Wang, X., Pu, W., Ren, Y., Zhang, X., Zhang, X., Shi, J., Jin, H., Dai, M. and Chen, Q.: Snow albedo reduction in  
482 seasonal snow due to anthropogenic dust and carbonaceous aerosols across northern China, *Atmos. Chem. Phys.*  
483 *Discuss.*, (September), 1–52, doi:10.5194/acp-2016-667, 2016.
- 484 Wang, Y., Ma, P.L., Peng, J., Zhang, R., Jiang, J.H., Easter, R.C., Yung, Y.L., 2018. Constraining aging processes of  
485 black carbon in the community atmosphere model using environmental chamber measurements. *J. Adv. Model.*  
486 *Earth Syst.* 10 (10), 2514e2526. <https://doi.org/10.1029/2018MS001387>.
- 487 Warren, S. G., and R. E. Brandt .: Optical constants of ice from the ultraviolet to the microwave: A revised  
488 compilation, *J. Geophys. Res.*, 113, D14220, doi:10.1029/2007JD009744, 2008.
- 489 Xu, B., Cao, J., Joswiak, D. R., Liu, X., Zhao, H. and He, J.: Post-depositional enrichment of black soot in snow-  
490 pack and accelerated melting of Tibetan glaciers, *Environ. Res. Lett.*, 7(1), 14022, doi:10.1088/1748-

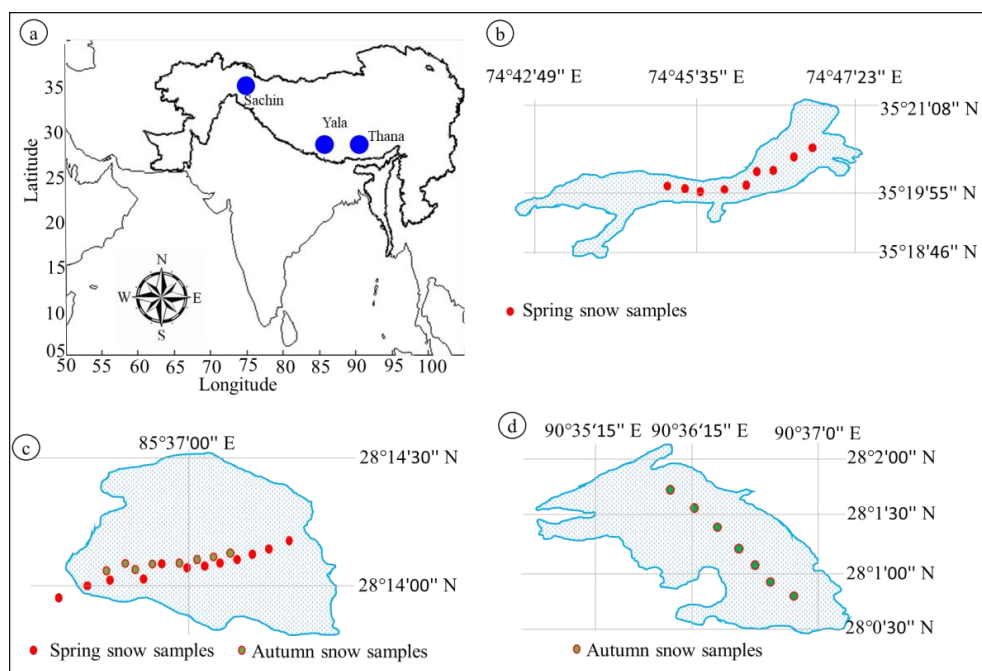


- 491 9326/7/1/014022, 2012.
- 492 Yang, S., Xu, B., Cao, J., Zender, C. S. and Wang, M.: Climate effect of black carbon aerosol in a Tibetan Plateau  
493 glacier, *Atmos. Environ.*, 111, 71–78, doi:10.1016/j.atmosenv.2015.03.016, 2015.
- 494 Yasunari, T. J., Koster, R. D., Lau, W. K. M., and Kim, K.: Impact of snow darkening via dust, black carbon, and  
495 organic carbon on boreal spring climate in the Earth system, *J. Geophys. Res.-Atmos.*, 120, 5485–5503,  
496 <https://doi.org/10.1002/2014JD022977>, 2015.
- 497 Yasunari, T. J., Bonasoni, P., Laj, P., Fujita, K., Vuillermoz, E., Marinoni, A., Cristofanelli, P., Duchi, R., Tartari, G.  
498 and Lau, K. M.: Estimated impact of black carbon deposition during pre-monsoon season from Nepal Climate  
499 Observatory - Pyramid data and snow albedo changes over Himalayan glaciers, *Atmos. Chem. Phys.*, 10(14),  
500 6603–6615, doi:10.5194/acp-10-6603-2010, 2010.
- 501 Yao, T., Xue, Y., Chen, D., Chen, F., Thompson, L., Cui, P., Koike, T., Lau, W. K., Lettenmaier, D., Mosbrugger, V.,  
502 Zhang, R., Xu, B., Dozier, J., Gillespie, T., Gu, Y., Kang, S., Piao, S., Sugimoto, S., Ueno, K., Wang, L., Wang,  
503 W., Zhang, F., Sheng, Y., Guo, W., , Yang, X., Ma, Y., Shen, S. S. P., Su, Z., Chen, F., Liang, S., Liu, Y., Singh, V.  
504 P., Yang, K., Yang, D., Zhao, X., Qian, Y., Zhang, Y., & Li, Q. (2019). Recent Third Pole’s Rapid Warming  
505 Accompanies Cryospheric Melt and Water Cycle Intensification and Interactions between Monsoon and  
506 Environment: Multidisciplinary Approach with Observations, Modeling, and Analysis, *Bulletin of the American*  
507 *Meteorological Society*, 100(3), 423-444. Retrieved Nov 1, 2021,  
508 from <https://journals.ametsoc.org/view/journals/bams/100/3/bams-d-17-0057.1.xml>
- 509 You Q., Z. Cai, Nick Pepin, Deliang Chen, Bodo Ahrens, Zhihong Jiang, Fangying Wu, Shichang Kang, Ruonan  
510 Zhang, Tonghua Wu, Pengling Wang, Mingcai Li, Zhiyan Zuo, Yanhong Gao, Panmao Zhai, Yuqing Zhang.  
511 Warming amplification over the Arctic Pole and Third Pole: Trends, mechanisms and consequences. *Earth-*  
512 *Science Reviews*, 217: 103625. <https://doi.org/10.1016/j.earscirev.2021.103625>.
- 513 Zaveri, R., Easter, R., Fast, J., and Peters, L.: Model for simulating aerosol interactions and chemistry (MOSAIC), *J.*  
514 *Geophys. Res.*, 113, D13204, doi:10.1029/2007JD008782, 2008.
- 515 Zhang, Q., Kang, S., Kaspari, S., Li, C., Qin, D., Mayewski, P. A., and Hou, S.: Rare earth elements in an ice core  
516 from Mt. Everest: Seasonal variations and potential sources, *Atmos. Res.*, 94, 300– 312, 2009.
- 517 Zhang, X. L., Wu, G. J., Kokhanovsky, A., Yao, T. D., and Tong D.: Spectral albedo parameterization for dirty snow  
518 with considering mirco-physicochemical properties of impurities - Part I: Theory and preliminary evaluation,  
519 2016
- 520 Zhang, Y., Kang, S., Xu, M., Sprenger, M., Gao, T., Cong, Z., Li, C., Guo, J., Xu, Z., Li, Y., Li, G., Li, X., Liu, Y.  
521 and Han, H.: Light-absorbing impurities on Keqikaer Glacier in western Tien Shan : concentrations and potential  
522 impact on albedo reduction, *Sciences in Cold and Arid Regions*, 9(2), doi:10.3724/SP.J.1226.2017.00097. 2017.
- 523 Zhang Y. L., S. Kang, M. Sprenger, Z. Cong, T. Gao, C. Li, S. Tao, X. Li, X. Zhong, M. Xu, W. Meng, B.
- 524 Neupane, X. Qin, M. Sillanpää. 2018. Black carbon and mineral dust in snow cover on the Tibetan Plateau. *The*  
525 *Cryosphere*, 12: 413-431. <https://doi.org/10.5194/tc-12-413-2018>.
- 526
- 527 Zhao, C., Hu, Z., Qian, Y., Ruby Leung, L., Huang, J., Huang, M., Jin, J., Flanner, M. G., Zhang, R., Wang, H., Yan,



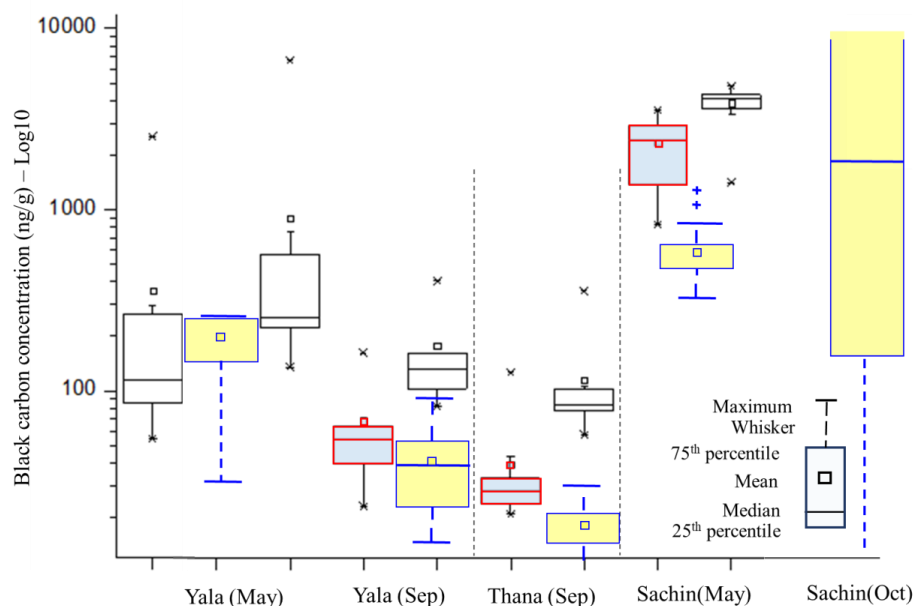
528 H., Lu, Z., and Streets, D. G.: Simulating black carbon and dust and their radiative forcing in seasonal snow: a  
529 case study over North China with field campaign measurements, Atmos. Chem. Phys., 14, 11475–11491,  
530 <https://doi.org/10.5194/acp-14-11475-2014>, 2014.  
531  
532





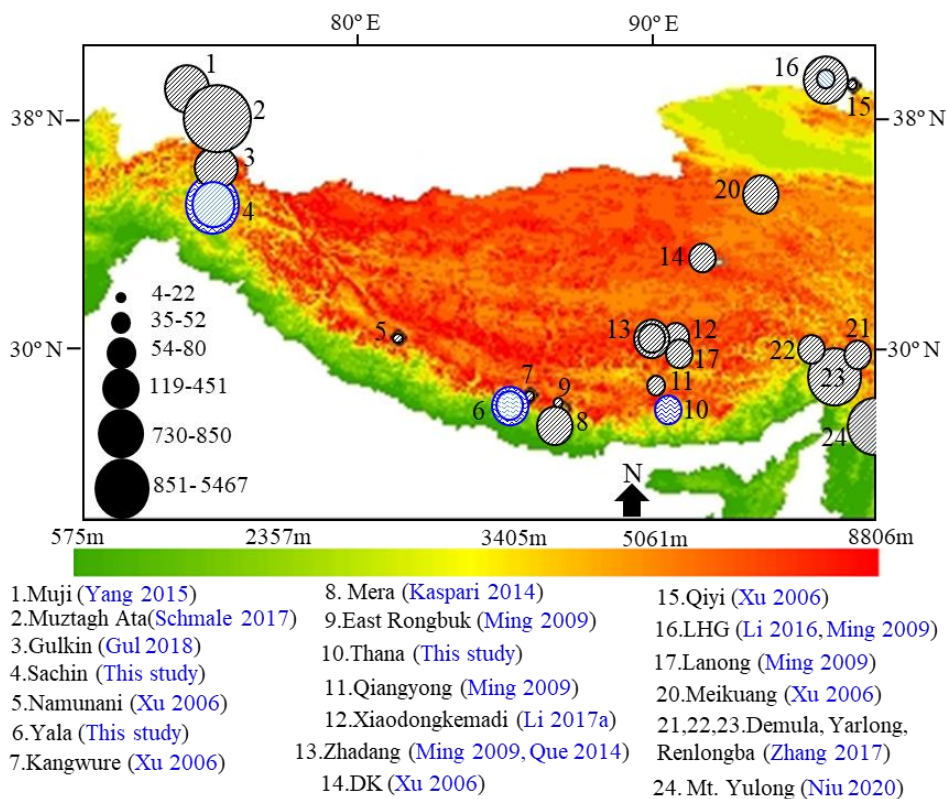
533  
 534  
 535  
 536

**Fig. 1.** Study area map (a) locations of selected glaciers in Himalaya Karakoram and Hindu Kush region (b) Sachin glacier in Pakistan (c) Yala glacier in Nepal (d) Thana glacier in Bhutan



537  
 538  
 539  
 540

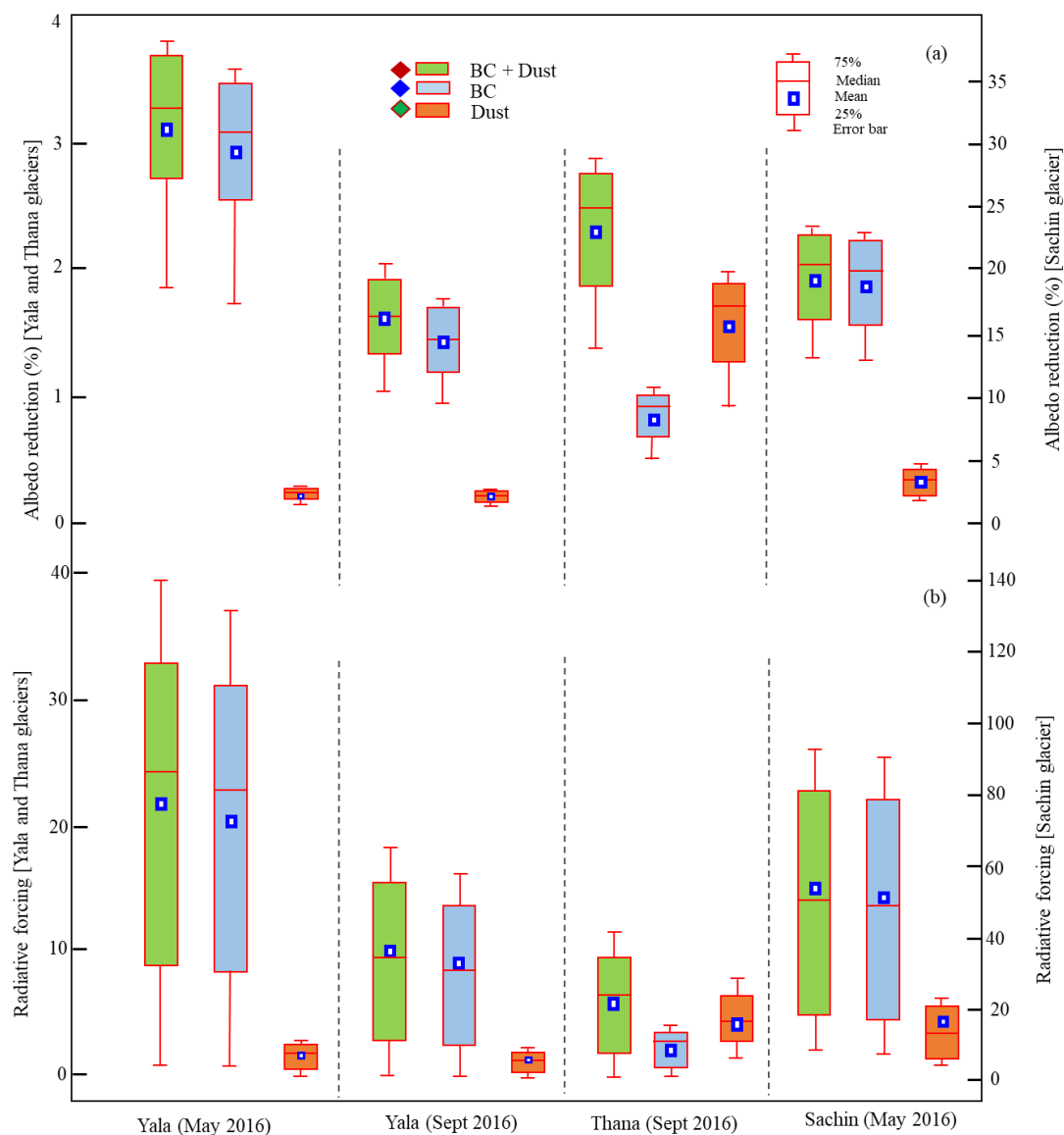
**Fig. 2.** Whisker plots of black carbon (red box) and organic carbon (black box) concentrations (ng/g) in snow samples collected from three different glaciers in spring and autumn 2016. The yellow boxes are representing BC content in surface snow from WRF-Chem simulations.



541

542 **Fig. 3. Black carbon concentrations (ng/g) in snow/ice samples in Himalayan, Karakoram and Tibetan Plateau in**  
 543 **previous studies (black circles) and this study (blue circles).**

544



545

546

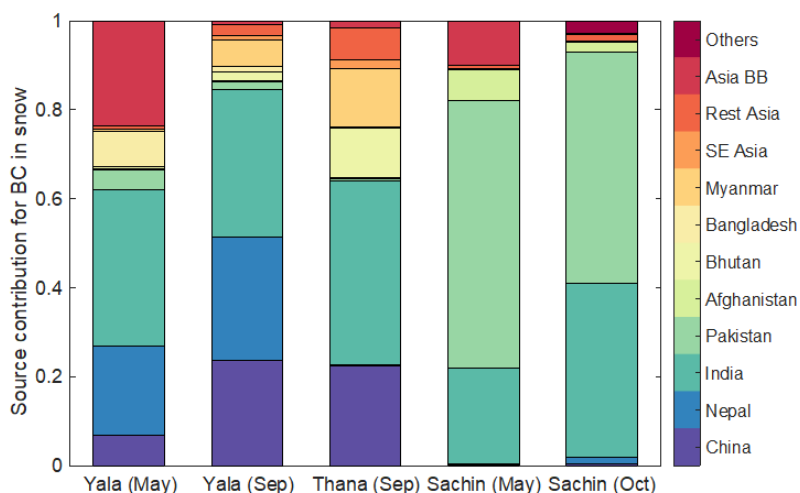
547

548

**Fig. 4.** (a) Snow albedo reduction due to black carbon, dust and combined (black carbon and dust) during day time for a range of solar zenith angles. (b) Average instantaneous radiative forcing based on albedo reduction values during day time.

549

550



551

552 **Fig. 5. Source contributions to BC content in surface snow from WRF-Chem simulations at the three measurement**  
 553 **glacier sites during the measurement periods. Source regions include anthropogenic emissions from China, Nepal,**  
 554 **Pakistan, Afghanistan, Bhutan, Bangladesh, Myanmar, Southeast (SE) Asia, and the rest of Asia, as well as Asian biomass**  
 555 **burning (BB) and BC transported from areas outside the study domain (Others).**

556

557

558

559 **Table 1. Snow sampling time and locations from selected glaciers**

Glacier	Lat/Long	Sampling date	Average elevation	Himalayas
Yala (Nepal)	28° 14' 12.25"N, 85° 37' 04.24"E	4 <sup>th</sup> - 7 <sup>th</sup> May 2016	4950 meters	Central
Yala (Nepal)	28° 14' 12.25"N, 85° 37' 04.24"E	29 <sup>th</sup> September 2016	4950 meters	Central
Thana (Bhutan)	28° 01' 22.23"N, 90° 36' 28.72"E	15 <sup>th</sup> September 2016	5400 meters	Central
Sachin (Pakistan)	35° 19' 55"N, 74° 45' 35"E	15 <sup>th</sup> May 2016	3230 meters	Western

560

561 **Table 2. Comparison of BC mass concentration, albedo reduction, radiative forcing and potential source regions of**  
 562 **pollutants for central and western Himalayan glaciers during the study period**

	Central Himalaya min – max (average)	Western Himalaya min – max (average)	Time period
Monthly mean temperature (°C)	2.05-14.36(10.35) Yala -9.11- 5.68(0.23) Thana	-10.78 - 14.63 (3.57) Sachin	Apr 2015- Oct 2017
Monthly mean precipitation (mm day <sup>-1</sup> )	0.04536 - 41.472 Yala 1.0195 - 50.112 Thana	0.1546 - 5.866 (Sachin)	Apr 2015- Oct 2017
Elevation of sampling location (meters)	4580-5675 (5127)	3134-3957(3545)	
Observed BC in surface snow (ng g <sup>-1</sup> )	21 – 2529 (~350)	835 – 3545 (~2300)	2016
Albedo reduction (%) due to BC particles in snow	0.13-3.82	12.00-24.00	2016
Instantaneous radiative forcing	0.0-39.65	0.03 to 96.48	2016



(W m<sup>-2</sup>) due to BC particles

Potential source regions of  
pollutants

3. WRF-Chem simulations

For the Yala site, it is dominated (>50%) by anthropogenic emissions from India and Nepal for both May and October, while the biomass burning contribution (>20%) increases largely in May. For the Thana site, it is dominated (>60%) by anthropogenic emissions from China and India in September, while anthropogenic emissions from Bhutan and Myanmar also contribute about 10%, respectively.

For the Sachin site, it is predominantly affected by anthropogenic emissions from India and Pakistan (total contribution >80%), while the spring biomass burning only contributes to ~10% in May.

563

564